https://doi.org/10.5194/wes-2025-216
Preprint. Discussion started: 10 December 2025

WIND ENERGY SCIENCE DISCUSSIONS
Open Access

Enhancing yaw control resilience in wind turbines with CFD-informed digital twins

Lorenzo Carrattieri[1], Carlo Cravero[1], Michele Marco Lanza[2], Michelangelo Mortello[2], Stefano Tedeschi[3]

[1]DIME, University of Genoa, Genoa, 16145, Italy
[2]Istituto Italiano della Saldatura, Genoa, 16141, Italy
[3]CDEM, Cranfield University, Cranfield, MK43 0AL, United Kingdom

Correspondence: Lorenzo Carrattieri (lorenzo.carrattieri@edu.unige.it)

Abstract. Wind turbines are pivotal in the transition towards renewable energy. The operational conditions of these machines are continuously monitored through sensors that measure key indicators of efficiency and performance, including yaw angles, rotational speed, and vibrations. However, sensors are subjected to wear, degradation and consequent reduction in data reliability over time, which provides scope for developing a consistent and effective method to detect misinterpretation of turbine operating conditions caused by faulty measurements.

This research presents a novel method that integrates Computational Fluid Dynamics (CFD) simulations into a Digital Twin (DT) model to detect and correct yaw misalignment caused by faulty wind direction readings. Yaw error is estimated by interpolation across CFD-based performance data using live sensor measurements. The novel DT-based method was validated through experimental testing on a small-scale horizontal-axis wind turbine.

The results provide scope for a significant improvement in the resilience of wind turbines under conditions of sensor malfunctions, without the need for human intervention or supervision.

The proposed method is intended to be adaptable, enabling analysis of diverse failure modes under varying operational conditions. This work also advances condition monitoring and sustainable asset management, offering potential for a larger adoption across different turbomachinery applications.

1 Introduction

In today's energy landscape, wind turbines play a crucial role in decreasing dependence on fossil fuels and addressing climate change (Bashir, 2022; Duranay et al., 2024; Veers et al., 2022). The wind energy sector is rapidly growing, with its share of global electricity generation expected to rise from 5 % to 30 % by 2050 (Arshad and O'Kelly, 2019; Farina and Anctil, 2022), consequently, large investigations are conducted to make sure that the utilization of these systems is exploited at its full potential, limiting factors that may compromise efficiency and effectiveness in energy production. Condition monitoring is critical for ensuring the reliable and cost-effective operation of wind turbines, leveraging both conventional signal processing methods and innovative big data analysis to support predictive maintenance strategies (Benbouzid et al., 2021; Khan and Byun, 2023).

Faulty sensors represent a significant risk to wind turbine performance by providing incorrect information and initiating ill-informed control measures. These errors can lead to various faults, including accelerated component wear, overheating, and rotor imbalance (Kini et al., 2023; Liu et al., 2022).

This paper focuses on one critical consequence of such sensor faults: yaw misalignment, with a specific focus on static yaw misalignment, which is a constant offset between the nacelle position and the actual wind direction. This type of misalignment often results from sensor-associated problems such as exposure to harsh environmental conditions, miscalibration, or software faults. Due to inappropriate alignment of the rotor with respect to the wind direction, yaw misalignment diminishes aerodynamic efficiency, decreases energy production, and increases structural loads on the turbine (Bao and Yang, 2021; Jing et al., 2020). In addition to the static case, yaw misalignment may also occur in a dynamic form, where the deviation between the nacelle orientation and the incoming wind direction varies over time. Dynamic yaw misalignment is primarily caused by the delayed response of the yaw control system to rapidly changing wind directions, resulting in transient misalignments that induce unsteady aerodynamic loads, power fluctuations, and additional fatigue stresses on the turbine structure (Gao and Hong, 2021; Wang et al., 2019). Yaw errors ranging from 4° to 20° can decrease the annual energy production by approximately 2.7 % to 11 % according to the size and design of the turbine (Astolfi et al., 2020; Hulsman et al., 2022; Liew et al., 2020; Yusong and Solomin, 2020). Previous research stated that acceptable misalignments should range from ±5° to ±10°, beyond which significant power losses and aerodynamic inefficiencies emerge (Cardaun et al., 2019; Simley et al., 2020).

Data-driven methods based on either Supervisory Control and Data Acquisition (SCADA) or Light Detection and Ranging (LiDAR) data offer scalable solutions for large-scale implementation to detect and compensate for static and dynamic yaw errors without the need for additional hardware (Chen et al., 2024; Gao and Hong, 2021).

For example, Gao and Hong (2021) propose a method for dynamic yaw misalignment correction using supervised machine learning trained on SCADA data. Their strategy estimates yaw error through the analysis of power deviations on a short-term horizon and has been shown to be effective under both static and dynamic yaw faults, given a large amount of training data. However, this approach requires the introduction of intentional faults into the system for model calibration and validation, which limits rapid and smooth scalability in actual wind farms.

Data-driven approaches inherently rely on the representativeness and on the quality of historical data, since these limit their own transferability to any unobserved fault. As an example of a poor-quality dataset, historical data could have been collected in the past by sensors that were affected by faulty conditions due to deterioration or being incomplete, or extracted from not sufficiently diverse training datasets (Badihi et al., 2022).

Digital Twins (DTs) are increasingly adopted as a tool to enable condition monitoring and establish a clear, complete, and time-controlled track to exploit data effectively. They integrate real-time operational data with virtual models of the turbine to provide more interpretable and reliable fault detection, while also supporting performance diagnostics and control optimization in wind energy applications (De Kooning et al., 2021; Momber et al., 2022; Stadtmann et al., 2023). Specifically, CFD-based DTs integrating real-time data with Computational Fluid Dynamics (CFD) models are increasingly recognised for their capacity to achieve condition-monitoring while introducing the fundamental physics laws underpinning the behaviour of the physical system. This is important for two main reasons: on one hand, it allows us to generate an accurate living DT in which a calibrated and high-fidelity fluid dynamic model is integrated and continuously affected by experimental and condition-related sensor datasets; on the other hand, a complete DT enables the access to a better engineering understanding and interpretation of the system operational conditions, especially when subjected to mismatch from expected performance (Kang et al., 2024; Solari et al., 2024)

In line with the above-mentioned potential, this paper proposes an innovative DT-based method capable of detecting and correcting yaw misalignment caused by faulty wind direction sensors. Unlike conventional data-driven approaches, the presented DT integrates condition monitoring parameters detected by the sensors with CFD-derived performance surfaces, without any need for prior training on faulty conditions. Yaw error is identified as an error only according to the outcome of the DT, without assuming prior determined misalignment data.

Once the DT was validated, its use could be demonstrated to control yaw misalignment due to sensor faults. As the wind vane sensor provides for the turbine rotor axis to be oriented towards the direction that enables maximum performance, its fault provokes the turbine rotor axis shifting towards a direction that compromises performance, resulting in a consequent mismatch between the expected turbomachine performance and condition monitoring data. The control action provided by the DT consists of being robust and capable of generating feedback data to correct the turbine rotor axis towards the wind flow direction, thereby optimizing the turbine's performance.

Even when sensors are not effective because of faults, the DT is capable of leveraging real-time wind sensor measurements and autonomously detecting and correcting erroneous yaw angles, significantly enhancing fault tolerance in turbine control systems. As a result, this solution presents a robust, scalable, and complementary solution to data-driven approaches, with high value in operational situations where sensor integrity, data availability, or environmental variability could undermine conventional machine learning-based systems. Finally, the DT-based solution established herein delivers a practical framework for driving digitalization strategies and resilience in wind energy operations.

2 Materials and methods

2.1 Experimental setup

For developing and testing the DT-based condition monitoring method, an experimental campaign was performed using a small-scale horizontal axis wind turbine (HAWT): Pikasola 400W-12V Wind Turbine Generator. The turbine is originally passively yawed by the wind thanks to its tail; it has a rotor with a diameter of 1.3 m, and it is characterized by a rated power of 400 W generated at 12 V DC. The rated rotational speed of 800 min^{-1} is reached for an incoming wind speed of 13 m s^{-1}, whereas power starts to be delivered for a cut-in speed of 2.5 m s^{-1}.

The turbine was tested outdoors at the airfield of Cranfield University, Bedfordshire, United Kingdom, located at a latitude of 52° 03' 59.5" N and longitude of 0° 37' 34.0" W. The tests were run during January and February 2025, where the registered average wind speeds ranged from 4 to 9 m s^{-1}, with wind gusts that reached 17 m s^{-1}. Figure 1 presents the generator installed on a 2.0 m long pole, which was equipped with a dedicated adjustable basement frame.

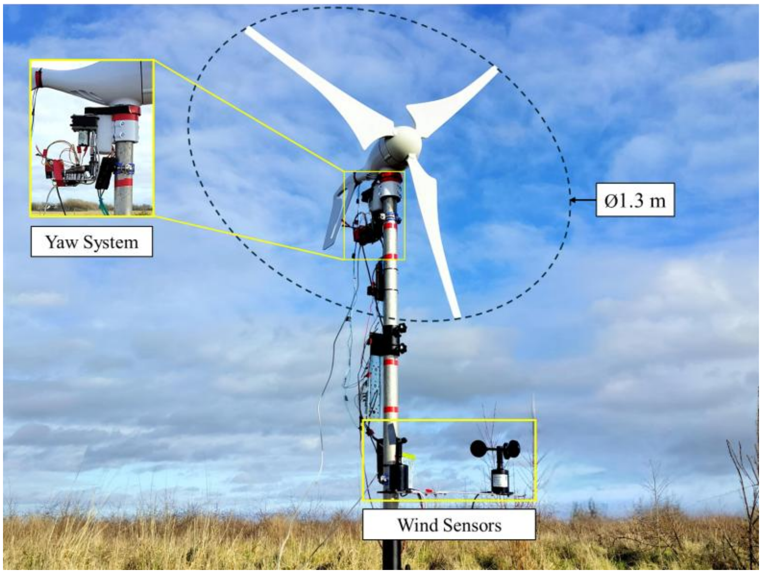

Figure 1. Small-scale wind turbine (Pikasola 400W-12V, 1.3 m rotor diameter) on a 2.0 m pole with dedicated base during outdoor testing at Cranfield University airfield, UK.

The experimental setup included a custom-built sensor network and yaw control system, installed on the asset to enable real-time monitoring and correction of yaw misalignment. Details of the array are provided in Sect. 2.3 and 2.4. Furthermore, the setup included specifically dedicated sensors to enable the measurement of the turbine's aerodynamic performance using two dimensionless parameters, which will be defined and further discussed in detail in Sect. 2.2.2: the power coefficient (Cp) and the tip speed ratio (TSR).

2.2 CFD modelling

2.2.1 Geometry and domain

The machine geometry was developed as a computer-aided design (CAD) model. In particular, the blade geometry was extracted from a previous model already developed by Utah Valley University (Shakya et al., 2024), since previous research had already been conducted on the same specific turbine; the nose and the nacelle of the wind turbine generator were designed by reverse engineering from the physical asset. Simplifications included not modelling the wind turbine's pole and tail, but only the rotor and its nacelle.

As presented in Fig. 2, the fluid domain consisted of a box space around the full rotor of size 5Dx5Dx12D, where D is the turbine diameter. The rotor was located 4 diameters distant from the inlet of the domain, followed by a conical subdomain, moving in solidarity with the blades, with a locally denser mesh to capture the near-wake flow structures and the onset of wake formation. This space sizing is consistent with recommendations and practices found in the literature (Siddiqui et al., 2019, 2022). It is a common practice to define the computational domain being sufficiently large to accurately capture the flow field around the rotor while minimizing computational timing and cost.

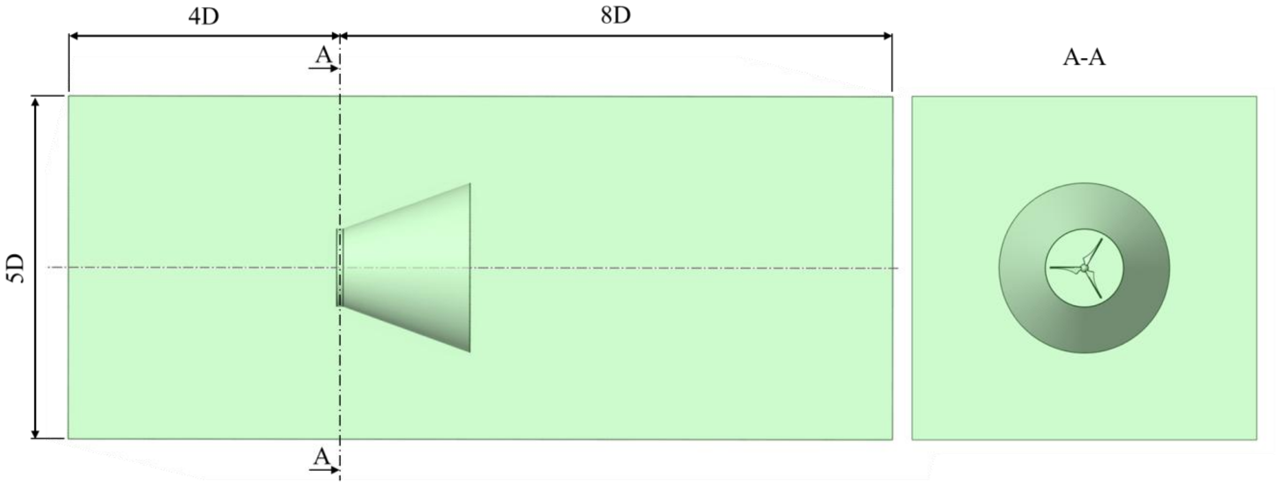

Figure 2. Overview of the CFD domain around the wind turbine rotor.

2.2.2 Simulation settings

Simulations were performed using the software Ansys Fluent 2024R1 on the Delta2 High-Performance Computing (HPC) cluster of Cranfield University. The Shear Stress Transport (SST) *k-ω* turbulence model was employed to compute the flow behaviour around the turbine under steady-state conditions. The choice of this model was due to its capacity to predict power output and aerodynamic loads more accurately than other Reynolds-Averaged Navier-Stokes equations (RANS) turbulence models, as commonly emphasised in literature (Al-Ttowi et al., 2024; Jha et al., 2024; Muiruri et al., 2019). The rotation of the rotor was modelled through a multiple reference frame (MRF) (ANSYS FLUENT 12.0 Theory Guide - 2.3.1 The Multiple Reference Frame Model).

Boundary conditions included a uniform inlet velocity with a turbulence intensity of 5 %. The simulated wind speeds were U_∞ = 3, 5, 8, and 13 m s^{-1}, in order to cover an incoming inflow that ranged from the cut-in speed to the rated speed of the selected wind turbine. Yaw misalignment was reproduced by modifying the inlet flow angle relative to the turbine's rotor axis by a yaw error angle, γ. When simulating yaw misalignment states, two faces of the box-shaped domain were set as inlets, whereas the opposing two downstream faces were set as pressure outlets. The top and bottom walls were configured as free-slip walls.

A common theoretical assumption is that yaw misalignment results in a symmetric power loss for positive and negative yaw errors (Lu et al., 2023). After verifying this hypothesis on power production, only positive yaw misalignment angles were tested, specifically at yaw errors γ = 5°, 10°, and 15°.

As anticipated in Sect. 2.1, the aerodynamic performance of the rotor was evaluated in terms of two standard dimensionless coefficients: the power coefficient (Cp) and the tip speed ratio (TSR), defined as:

$$C_p = \frac{P}{\frac{1}{2}\rho A U_\infty^3}, \tag{1}$$

$$TSR = \frac{\omega R}{\mathrm{U}_\infty}, \tag{2}$$

where P is the mechanical power extracted by the turbine, ρ is the air density, A is the area of the rotor disc, U_∞ is the wind speed, ω is the angular speed of the rotor and R is the radius of the turbine. These coefficients define the operating point of the turbine and were computed for both CFD simulations and following experimental measurements.

CFD simulations were conducted for each selected wind speed, with the rotor speed adjusted to achieve the target TSR, ranging from 2 to 8 (Lu et al., 2023; Siddiqui et al., 2019). Aerodynamic power was calculated by multiplying the rotor torque by the prescribed rotational speed once it reached full convergence.

The computational mesh was designed to be polyhedral and unstructured, consisting of approximately 31 million elements, with a blade first layer thickness of 1.22e-5 m that granted a y+ value of about 1 for the analysed operations. Although a systematic mesh independence study was not conducted, the mesh resolution was chosen based on prior CFD experience from similar applications (Carrattieri et al., 2025; Cravero et al., 2025), ensuring precise near-wall treatment and stable convergence.

2.2.3 Estimation of yaw misalignment from CFD-derived performance data

The aerodynamic power response of the wind turbine was derived through CFD simulations introduced in the previous Sect. 2.2.2. For each specified yaw misalignment angle (γ = 0°, 5°, 10°, 15°) and for each prescribed wind speed (U_∞ = 3, 5, 8, 13 m s^{-1}), Cp-TSR distributions were collected from steady-state simulations in the specified range of TSR (2 to 8), amounting to a total of 112 simulations; this dataset was then used to develop a Cp-TSR-γ performance space.

For wind speeds of 8 m s^{-1} and 13 m s^{-1}, the Cp-TSR distributions showed the same aerodynamic behaviour due to aerodynamic similarity, with a relative percentage error below 5 %. Therefore, it was considered acceptable to select a single average dataset to represent the range of wind speeds from 8 to 13 m s^{-1} (see results in Sect. 3.1).

Due to computational limitations related to the extensive time required for each high-fidelity simulation, simulating the full range of yaw and TSR combinations across additional wind speeds was prohibitively expensive in terms of both CPU hours and storage. Hence, linear interpolation among the selected wind speeds was employed to generate Cp-TSR-γ data at intermediate wind speeds (U_∞ = 4, 6, 7 m s^{-1}).

The CFD-derived performance space was used as the foundation for the performance estimation and inference of the yaw misalignment $\gamma = f(Cp, TSR, U_\infty)$, as part of the virtual object of the DT model. Specifically, for each reference wind speed U_∞, a piecewise cubic interpolant was constructed over the (Cp, TSR) input space using scipy.interpolate.griddata from the SciPy library (Virtanen et al., 2020), allowing the retrieval of the corresponding yaw misalignment angle γ during

https://doi.org/10.5194/wes-2025-216
Preprint. Discussion started: 10 December 2025

experimental testing through direct measurements of Cp and TSR (see Sect. 2.6). For wind direction changes exceeding the maximum yaw offset simulated in CFD, the inference output was set to $\gamma = 15°$.

2.3 Sensor network and data flow

To monitor the wind turbine performance during experimental trials, the following sensors were used to sample data through an Arduino Yun microcontroller:

- Wind vane: RS-FXJT-V05-360 model;
- Anemometer: RS-FSJT-NPN model;
- Tachometer: A3144 from Allegro;
- Current sensor: ACS712ELCTR-30A.

An overview of the designed sensor network and the resulting data flow among the different modules is presented in the schematic of Fig. 3. Data from all sensors was collected at a frequency of 1 Hz and stored in a cloud MongoDB database (MongoDB Atlas | The Modern, Multi-Cloud Database |) via a custom Python script. The adopted sampling frequency was chosen according to the recommendations from the IEC 61400-12 standard for wind measurement systems, which suggests 1 Hz for proper accuracy (INTERNATIONAL ELECTROTECHNICAL COMMISSION, 2022).

The anemometer and wind vane were positioned 0.65 m above ground level; both were placed 0.3 m ahead of the rotor plane to minimize aerodynamic interference from the blades. A 0.4 m separation between the sensors ensured negligible mutual interference, with the configuration's suitability validated through CFD postprocessing. While the sensor arrangement is nonstandard relative to IEC-specified meteorological tower spacing (INTERNATIONAL ELECTROTECHNICAL COMMISSION, 2022), it was sufficient for local flow characterization and yaw correction under the specific constraints of small-scale, portable wind turbine testing.

The A3144 Hall effect sensor was used as a tachometer to measure rotor speed through three magnets attached behind each blade's root; the sensor was positioned right after the rotor to easily detect a full revolution. A custom Arduino routine processed the pulses to calculate the rotational speed. To measure the wind generator voltage, a voltage divider was implemented to scale the maximum possible voltage (12 V) to 5 V, compatible with the Arduino microcontroller.

A 12 V (55 W) halogen bulb was connected to the turbine as a fixed resistive load to maintain stable electrical performance, limiting the maximum current draw from the generator and resulting in lower total extractable power than the turbine's rated capacity. Nevertheless, this setup was sufficient to monitor relative power trends and validate the yaw correction logic within the DT model.

DC power was calculated by multiplying the current measured by the ACS712 current sensor and the voltage read through the voltage divider.

The entire sensor network was designed to be compact, allowing for outdoor deployment in varying locations without the need for fixed infrastructure. This flexibility enabled prompt repositioning of the turbine in open field conditions, facilitating experimental tests under naturally fluctuating wind conditions.

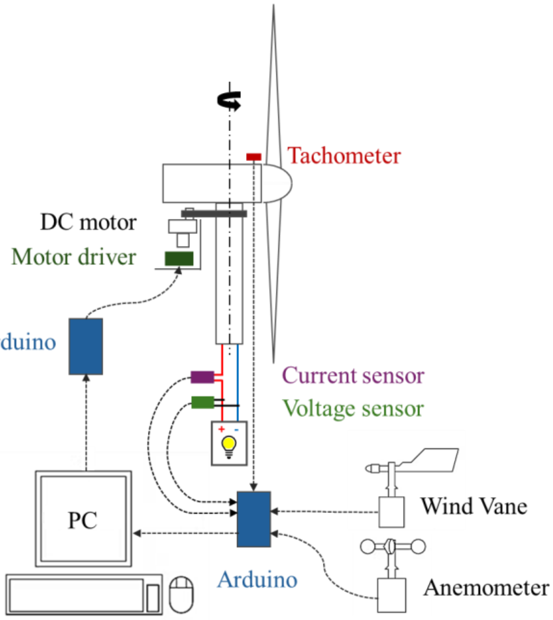

205 **Figure 3.** Schematic of the sensor network and data acquisition system for the instrumented wind turbine.

2.4 Yaw control system

A custom yaw control system was developed to adjust and correct the turbine's yaw angle. Yaw actuation was built using a Crouzet 82840 (Gear Ratio = 750) brush DC motor connected to the nacelle via a belt drive and controlled using an Arduino Uno microcontroller together with the BTS7960 motor driver module (see Fig. 3). The motor shaft was fitted with a 35 mm-diameter pulley that, via a 5 mm-pitch belt, drove a 75 mm-diameter pulley mounted on the nacelle shaft. The pulley axes were spaced 80 mm apart.

This design ensured sufficient robustness to overcome gyroscopic forces from rotor rotation and system friction. The system was manually calibrated to ensure accurate yaw actuations with a yaw speed of 1 ° s^{-1}. Calibration was performed by tracing visible markers around the nacelle shaft, allowing angle adjustments to be verified against known reference positions.

2.5 Numerical-experimental power matching

To ensure consistency between the power output of the wind generator and the aerodynamic predictions derived from CFD simulations, a three-step correction technique was employed. Consistency between experimental tests and numerical simulations was necessary to grant accurate real-time monitoring within the DT feedback logic for proper CFD interpolation.

First, similarly to the approach described in Sect. 2.2.3, a piecewise cubic interpolant was designed over the CFD-derived Cp values corresponding to the correctly aligned (i.e., non-misaligned) yaw condition. The interpolation was performed in the (TSR, U_∞) space to estimate the expected power coefficient Cp for any future measured operating point. The results of the interpolation are provided in Sect. 3.2.

https://doi.org/10.5194/wes-2025-216
Preprint. Discussion started: 10 December 2025

Second, instantaneous experimental values for TSR and U_∞, obtained during the second turbine trial (see Sect.2.7), were then fed into the interpolator to find the predicted Cp according to CFD. Before interpolation, outlier filtering was applied to each experimental time series using the interquartile range (IQR) method (threshold = 2.5).

Therefore, a correction factor (CF) dataset was determined as the pointwise residual difference between interpolation-predicted and experimentally obtained Cp values under the same measured TSR and U_∞:

$$CF\left(TSR^{exp}, U_\infty^{exp}\right) = Cp^{CFD}\left(TSR^{exp}, U_\infty^{exp}\right) - Cp^{exp} \tag{3}$$

Where the superscript exp stands for the experimentally measured values, whereas CFD refers to the interpolated values extracted from CFD results.

In a third step, a cubic spline model was fitted to the pointwise CF values, with the smoothness parameter s equal to 1, to create a correction surface mapping the (CF, TSR, U_∞) space (see Sect. 3.2).

This method allowed for the compensation of differences due to sensor noise, unmodeled losses, and mechanical-electrical conversion inefficiencies. Nevertheless, the interpolation built upon correctly yawed data was also used as a first approximation for correcting yawed operating conditions, under the assumption that yaw misalignment introduced no drastic change in conversion losses other than the aerodynamic Cp reduction itself (Astolfi et al., 2023; Lu et al., 2023).

As a result, in subsequent experimental trials for each set of measured TSR and U_∞, a correction factor was computed by interpolating the cubic spline model and summed to the measured Cp to obtain a corrected power coefficient within the range of the CFD values, ready for processing by the DT model.

2.6 Digital twin model for yaw fault detection and correction

The DT model was specifically designed to guarantee that the turbine was continuously aligned with the wind inflow. If misalignment was detected, the condition-based logic of the model's algorithm identified whether the issue stemmed from a change in wind direction or from faulty wind vane data. The system operated in a closed loop, with right-time feedback and self-correcting yaw adjustments based on sensor data and CFD interpolation.

To distinguish the sign of yaw misalignment, yaw error was defined as positive when the wind direction deviated clockwise from the rotor axis (looking down from above), placing the wind vector on the right-hand side of the rotor axis when viewed from upstream.

The DT control logic was written in Python. Temporal data was fetched from the cloud database with a sampling interval of 30 s; this interval was partly constrained by the MongoDB data retrieval latency, which extended the loop duration to approximately 32 to 33 s.

Outlier filtering was then applied to each time series using the IQR method (threshold = 2.5). Cp and TSR time series were computed following the definitions provided in 2.2.2. A correction factor was then summed to each fetched Cp value to be consistent with the CFD performance results after interpolating the cubic spline model presented in Sect. 2.5.

Subsequently, the averaged values of TSR, wind speed, and the corrected Cp over the sampling interval were used as inputs for the right-time γ inference model. As explained in Sect. 2.2.3, the model works based on a piecewise cubic interpolation of the CFD-derived performance space, returning a yaw misalignment angle γ = f(Cp, TSR) for the selected wind speed U_∞. Before interpolation, the wind speed average was rounded to select the closest corresponding response surface.

To check for the presence of a yaw fault caused by faulty sensor data and to resolve the sign ambiguity of yaw misalignment under potentially faulty wind vane conditions, the DT model implemented a self-correcting feedback logic, with a threshold for yaw fault detection set to 5°. The control loop continuously monitored the percentage change in the Cp across two consecutive time intervals and the inferred yaw error γ. For each time interval, the Cp percentage change was calculated as follows:

$$Cp\ percentage\ change = \frac{Cp_i - Cp_{i-1}}{Cp_{i-1}} * 100\ [\%] \tag{4}$$

where i is the current time interval.

Yaw fault from wind data was flagged only if the Cp percentage change decreased for two consecutive loops and the inferred γ exceeded the defined threshold. The logic initially assumed a positive yaw misalignment (clockwise deviation) and applied a corresponding yaw correction through the yaw system. Based on the aforementioned conditions:

- If the inferred γ in the previous interval was less than the threshold, the controller proceeded to apply a clockwise correction by adding the current γ to the current yaw angle. This tested the hypothesis of a positive yaw error.
- Conversely, if the γ from the previous interval was already greater than the threshold, the control logic concluded that the original correction was in the wrong direction, indicating a negative yaw misalignment. In this case, a stronger counterclockwise correction was made by subtracting twice the previously inferred γ from the current yaw angle.

This process enabled the DT model to actively diagnose the sign of the yaw error through direct feedback over consecutive time intervals. If the power output worsened after assuming a positive yaw misalignment, the model's algorithm was capable of detecting and correcting the course by inferring a negative yaw deviation.

In the absence of inferred faults, the wind vane sensor data were considered to be correct, and the control logic operated to adjust the yaw angle of the turbine to be aligned with the measured wind direction. To ensure a consistent response, a control flag was implemented in the algorithm to disable further actuations linked to the healthy sensor state once a faulty sensor state was detected. As a result, the turbine's yaw angle adjustments relied only on CFD interpolation, maintaining alignment with the wind direction even in the presence of unreliable sensor data. In this configuration, the CFD interpolation itself acted as a virtual sensor, providing yaw measurements otherwise provided by the faulty device.

The adjustment command was sent through a dedicated Python interface, which actuated the 24 V DC motor driving the yaw system. The motor's movement was bounded between 110° and 230°, ensuring mechanical safety.

The loop then ran for 30 seconds (the defined sampling interval) before fetching a new set of data and calling the control logic and interpolation once again. During experimental testing, the DT model was manually interrupted, after which the motor drove the turbine to a neutral 180° reference position, providing a mechanical reset to the system with a safe shutdown.

2.7 Testing and validation procedures

To validate the proposed DT-based method, a three-phase experimental campaign was conducted using the setup described in Sect. 2.1. The turbine was tested outdoors under naturally fluctuating wind conditions, with each trial targeting a specific development objective.

First Trial - Data acquisition and streaming verification

The first trial aimed to verify real-time acquisition and cloud storage of sensor data. Sensor values (voltage, current, wind speed, direction and rotational speed) were streamed at 1 Hz and successfully stored in the cloud database. Wind speed and direction data were used for inflow characterization, rotational speed for tip speed ratio calculation, current and voltage for electrical power estimation. This data laid the foundation for deriving Cp and TSR in later trials. Wind data logged in this trial indicated outliers due to natural turbulence, which encouraged implementing IQR filtering.

Second Trial - Electromechanical power characterization

A second experimental session took place outdoors at the airfield of Cranfield University (see Sect. 2.1) to measure the electrical power output under actual loading conditions for the correctly yawed turbine. During the second trial, the turbine was left to be passively yawed by the wind. From current and voltage measurements, the electromechanical Cp could be calculated and compared against the aerodynamic Cp derived from CFD simulations. A notable deviation resulted from this comparison due to conversion losses as well as to limitations in electrical load capacity.

A CFD-calibrated correction factor (CF), as a function of the turbine operating point, was established to adjust the measured Cp to an estimated aerodynamic Cp. This correction allowed for meaningful calibration between experimental data and the CFD-derived performance results used in the following DT model (see Sect. 2.5).

Third Trial - DT validation and fault detection

The final trial tested the ability of the proposed method to detect and correct yaw misalignment. During this phase, in addition to the standard signals (wind speed, wind direction, power, rotational speed), the estimated yaw error γ, the measured yaw position, and the Cp trend were computed at every time interval. These parameters were used by the DT to detect misalignments and decide whether to override faulty wind direction readings. The trial consisted of four sub-tests:

1. Test 1, validation of yaw system actuation: A test of the customized yaw system of the turbine that validated its ability to align the rotor with the wind direction at each sampling interval.
2. Test 2, positive yaw misalignment: A yaw misalignment of +10° was established by subtracting 10° from the wind vane measurements before running the test. The DT model correctly sensed the misalignment through decreased

performance and successfully aligned the turbine with the real wind direction, circumventing the faulty sensor after the deviation had been confirmed. At the end of the second trial, the DT was also capable of detecting an average change in the wind direction.

3. Test 3, positive yaw misalignment: A repeat test with a +10° offset was performed; in this test, however, the DT did not measure the misalignment. The likely reason was increased turbulence and high-frequency gusts that temporarily obscured a degradation in the performance that is being relied on for detection.
4. Test 4, negative yaw misalignment: A negative yaw misalignment of -15° was simulated by adding +15° to the measurements of the wind vane before running the test. The DT model correctly sensed the fault from the interpolated CFD performance space and computed the proper yaw correction command.

Although these results demonstrated the promise of the DT in independent fault detection and fault correction, the system also tended to be sensitive to wind turbulence and inhomogeneities near the ground. These phenomena are omnipresent in the boundary layer of the atmosphere and can induce spurious corrections. Such effects should be weaker in utility wind turbines operating at higher hub heights, where wind profiles are more even.

3 Results and discussion

3.1 CFD calibration and integration within the digital twin framework

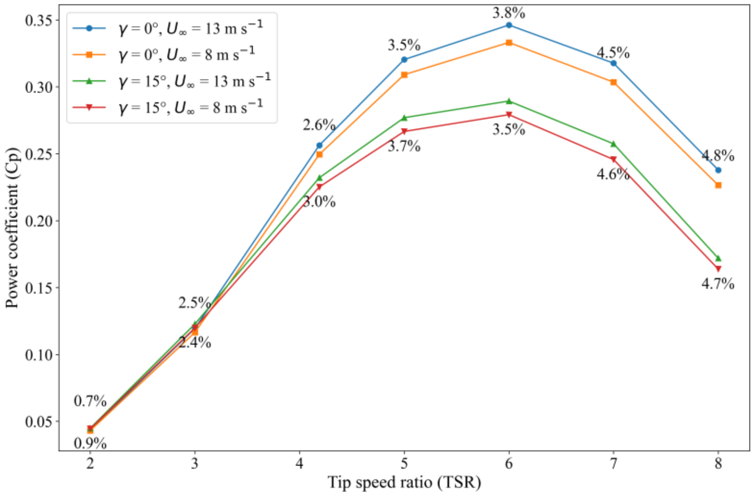

Figure 4. Cp-TSR curves for $\gamma = 0°$ and $\gamma = 15°$, at wind speeds of 8 m s^{-1} and 13 m s^{-1}. Relative deviations from the 13 m s^{-1} baseline are illustrated, confirming aerodynamic similarity across this range.

Figure 4 illustrates the Cp distributions against the TSR under various inflow conditions. Distributions for two wind speeds (8 m s^{-1} and 13 m s^{-1}) are presented under aligned ($\gamma = 0°$) and misaligned ($\gamma = 15°$) conditions. Relative deviations from the reference case at 13 m s^{-1} are marked on each curve.

The results confirm that in the TSR range from 2 to 8, the aerodynamic performance of the rotor is almost identical in terms of wind speeds. In any yaw angle error, the relative difference in Cp between 8 m s^{-1} and 13 m s^{-1} is less than 5 %, highlighting the aerodynamic similarity between the results. This feature supports the selection of modelling the wind turbine's aerodynamic performance, in the inflow range of 8 to 13 m s^{-1}, with a single averaged performance curve per yaw direction. This choice reduces the DT's inference problem dimensionality without sacrificing physical accuracy.

Figure 5 represents the aerodynamic power performance obtained from CFD calculations (white markers) in terms of Cp, TSR, yaw angle error γ, and wind speed U_∞. Results associated with the same incoming wind speed are fitted with a response surface, which varies in colour in terms of Cp. The yaw misalignment axis shows only positive deviations.

No direct experimental validation of the CFD calculations was conducted through wind tunnel or high-precision aerodynamic testing, but rather, was ensured through the addition of a correction factor (CF) defined through the second experiment (see Sect. 2.5).

In the figure, it is possible to observe the averaged performance surface representing the wind speed range over which aerodynamic similarity holds. Moreover, for every surface, there is an evident decreasing trend in the power response of the turbine when moving to greater yaw misalignment angles, as also shown in the literature (Lu et al., 2023). For wind speeds between 13 m s^{-1} and 5 m s^{-1}, the maximum power extraction was found at TSR equal to 6 under correct yaw conditions. For the 4 m s^{-1} and 3 m s^{-1} surfaces, the maximum Cp moved between TSR equal to 5 and 6.

Superimposed on the surface are indicative arrows showing the γ inference process. Namely, through sensor-based estimations of Cp, TSR, and U_∞, the DT model identifies the corresponding distribution associated with the averaged rounded value of wind speed and performs an interpolation to estimate the yaw misalignment angle γ. The figure enhances the physics underlying the DT model.

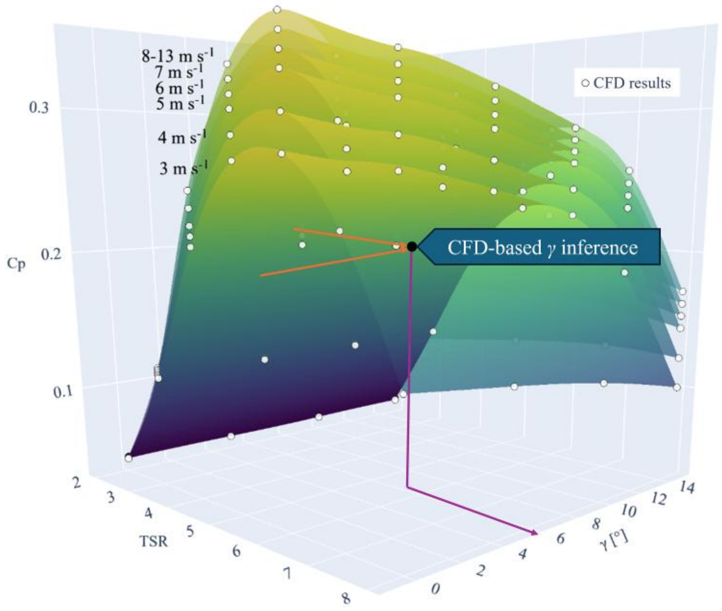

https://doi.org/10.5194/wes-2025-216
Preprint. Discussion started: 10 December 2025

Figure 5. CFD-derived performance surfaces showing Cp as a function of TSR, yaw misalignment γ, and wind speed. Arrows illustrate how the DT infers yaw error using real-time sensor inputs.

The CFD results for the rated wind speed of 13 m s^{-1} showed that the yaw-induced power degradation followed a cosine-based loss pattern with a TSR-dependent exponent. To quantify the yaw-induced power loss trend, the power output at various yaw errors was fitted to the classical cosine-exponent model (Lu et al., 2023), expressed through Eq. (5):

$$P(\gamma) = P_0 \cos^n(\gamma) \tag{5}$$

Where P_0 is the power extracted for the turbine properly aligned with the wind and n the exponent governing the power drop. A linear regression of $\log(P(\gamma)/P_{0)})$ versus $\log\,(cos(\gamma))$ was used to estimate the best fit exponent n, following the approach in yaw sensitivity modelling. As shown in Table 1, the exponent increased with TSR, ranging from -0.94 at TSR = 2 to 8.93 at TSR = 8, with the rated operating point of the small-scale turbine being represented by TRS = 4.19. This trend confirms the nonlinearity of yaw sensitivity with operating conditions and further supports the fidelity of the aerodynamic model.

Table 1. Cosine law exponent characterizing yaw-induced power loss at each TSR for rated wind speed (13 m s^{-1}).

TSR	n exponent
2.00	-0.94
3.00	-0.65
4.19	2.80
5.00	4.10
6.00	4.97
7.00	5.77
8.00	8.93

3.2 Experimental power correction results

Figure 6 illustrates the wind turbine performance surface calculated by CFD for aligned conditions (γ = 0°), with black markers indicating the original simulation data. As described in Sect. 3.1, one single average Cp-TSR curve was taken to describe the behaviour of the turbine for wind speeds from 8 to 13 m s^{-1}, based on accepted aerodynamic similarity.

This database was used as the basis to develop a correction factor (CF) that would align electromechanical readings with numerically predicted aerodynamic performance, described in Sect. 2.5. The resulting interpolating surface, overlaid on the original CFD data points, confirms a good agreement within the defined operating envelope.

https://doi.org/10.5194/wes-2025-216
Preprint. Discussion started: 10 December 2025

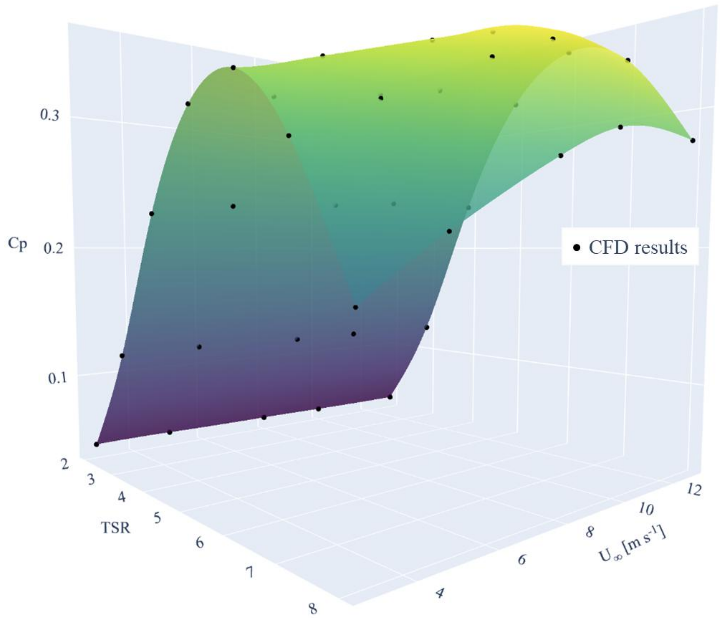

Figure 6. CFD-derived performance surface for the correctly yawed turbine (γ = 0°).

Figure 7 presents the computed CF datapoints, defined as the pointwise residual difference between the experimental Cp values and those interpolated from the CFD surface of Fig. 6, following Eq. (3). The CF values were used to build a smooth cubic spline model to estimate the aerodynamic Cp from electromechanical readings and to enable the DT algorithm to perform right-time adjustments.

The correction data gathered during the second experimental trial showed a banded distribution, corresponding to discrete operating conditions reached during testing. After IQR-based outlier removal, the dataset contained wind speeds between 2.5 m s^{-1} and 11 m s^{-1}, and TSR between 2 and 4.

The fitted spline exhibits a definite positive gradient in CF with increasing U_∞ and TSR. The trend shows larger discrepancies for greater TSR and U_∞ values between experimental and CFD-based Cp values, most likely due to increased rotational speeds and unaccounted electrical losses.

The developed correction model allows the DT to balance field measurements and CFD predictions to achieve consistent performance inference and fault detection.

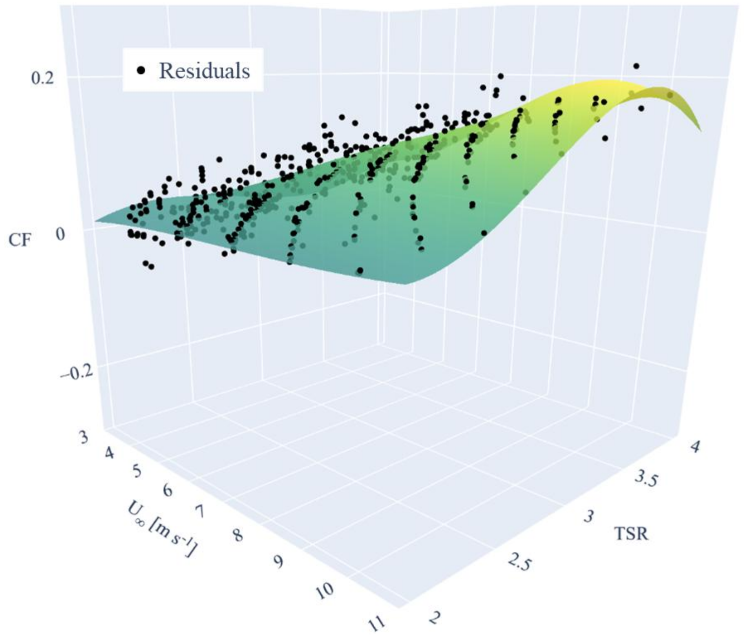

Figure 7. Correction factor (CF) values derived from the pointwise difference (residuals) between experimental and CFD-based Cp results.

3.3 Yaw fault detection performance

Figure 8 presents the outcome of Test 1, which was designed primarily to check the real-time responsiveness of the modified yaw actuation system under dynamic inflow conditions. Variable wind conditions were registered during the test. The turbine yaw angle was first initialized at 180°; as observed in the first panel, the DT model effectively changed the yaw direction of the turbine in each loop in line with the wind direction readings. Rapid changes in the wind direction occurred during the test, with values up to -18°. The DT model captured these changes, reflected in the Cp and TSR parameters, inferring yaw misalignment angles of 15° and 10° as shown in the second panel.

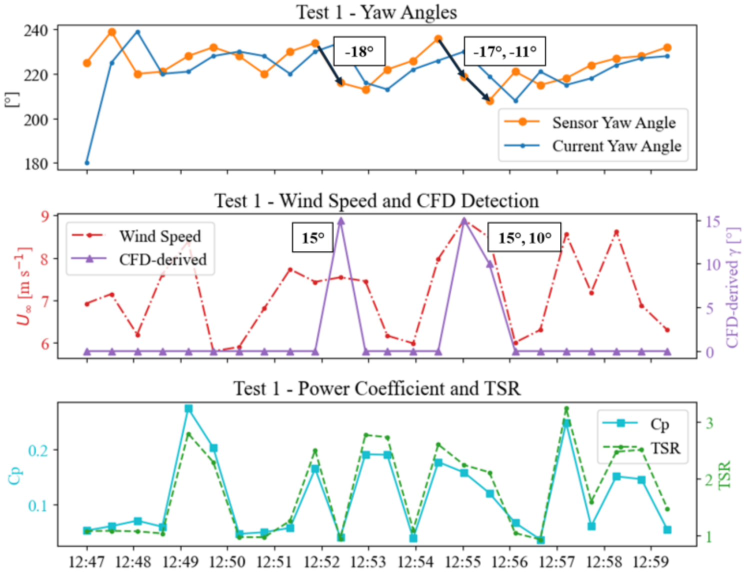

Figure 8. Time series from Test 1: verification of the yaw actuation system and initial DT fault inference under gusty conditions.

This observation indicates that DT could potentially monitor fast changes in wind direction and Cp. Furthermore, the analysis demonstrated that misalignment detection is more likely to occur during conditions of high wind strength, which led to greater TSRs and increased the responsiveness of the aerodynamic model.

Test 2 results are shown in Fig. 9. The test started with a -10° artificial bias in the wind vane readings, inducing a positive yaw misalignment of 10°. A 13° error was detected by the DT model at time 13:14:09 after about 3 minutes and corrective feedback was sent at the end of the loop, marked with a vertical dashed grey line. Due to the system's mechanical inertia, a second 9° error was detected in the subsequent loop, but no actuation was performed because of a Cp increase of 112 % following the first actuation.

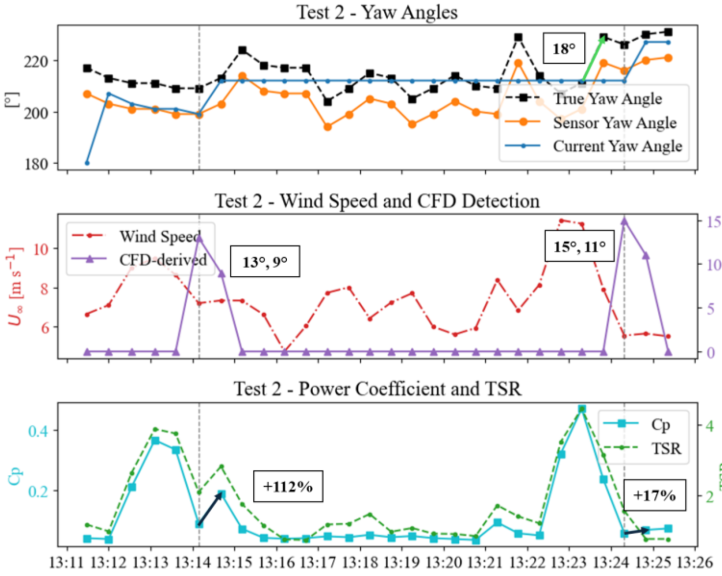

Figure 9. Time series from Test 2: detection and correction of a 10° yaw misalignment.

In addition, the first panel shows the real wind direction (marked in black) that the system adjusted to after the corrective feedback provided by the DT. Additionally, a strong wind direction change (+18°) was inferred close to the end of the test, which was picked up by the DT as a 15° deviation in the subsequent interval, providing a corresponding feedback action. A partial recovery of Cp (about 17 %) ensued and prevented a second feedback command. This reaction further illustrates the system's capability to adapt to changing inflow conditions and the CFD inference as a virtual sensor; the DT did not issue any unnecessary actuation commands, demonstrating robustness against false positives under gusty conditions.

In Fig. 10, the results for Test 3 are presented. For this type of test, a newly positive yaw misalignment fault of 10° in the wind vane readings was tested right from the beginning. In this case, although at time 13:33:36 the DT, through CFD interpolation, managed to detect a misalignment (12°), the system couldn’t provide feedback action due to the strong fluctuations in the wind inflow, which had a direct effect on the power production and could not satisfy the criteria at the base of the DT algorithm. This test was characterised by the lowest maximum wind speeds registered during the trial.

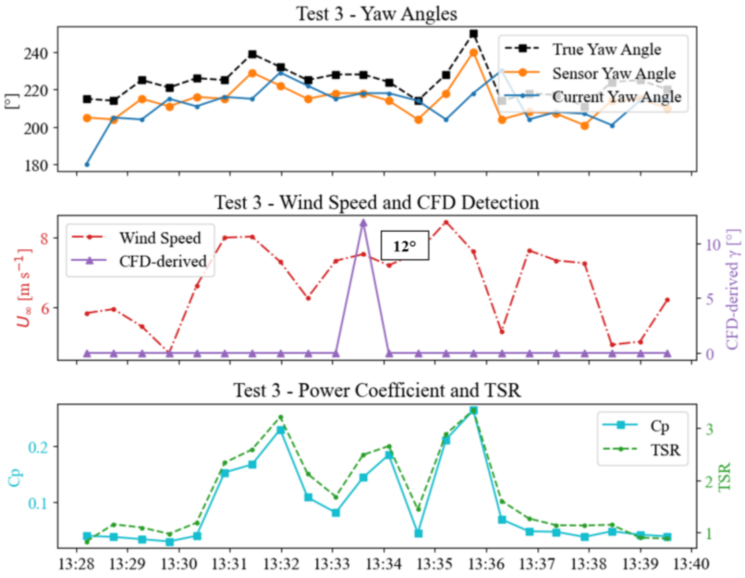

Figure 10. Time series from Test 3: fault detection under 10° misalignment suppressed by unstable inflow.

Figure 11 presents the results from Test 4 that concluded the third experimental trial. In this scenario, a negative yaw misalignment condition of 15° was simulated. Soon, from the beginning of the test, the twin signalled the presence of a misalignment, inferring a 14° yaw error. Only at time 13:49:36, after about 7 minutes, the algorithm could confirm the presence of a misalignment (+15°) and provide proper feedback, assuming it to be positive. It is possible to see that after the first feedback action, the registered Cp showed a -37 % decrease, which indicated to the algorithm that the provided actuation was in the wrong direction (positive clockwise), which was followed by another detection of 15° misalignment in the next loop. After the second detection, a second corrective actuation of -30° was issued; the corrective command resolved the negative yaw fault and successfully realigned the turbine with the wind inflow. This test highlighted the DT's ability to self-correct directional misclassification after detecting a post-actuation power drop.

In this case, Cp recovery in the time series was not very clear due to a rapid decrease in the wind speed that drove the turbine to TSRs close to 1. Although a modest increase in power can be seen following the correction, it is difficult to isolate this recovery from the effects of reduced inflow velocity. These trial outcomes directly informed the accuracy evaluation summarized in Sect. 3.4.

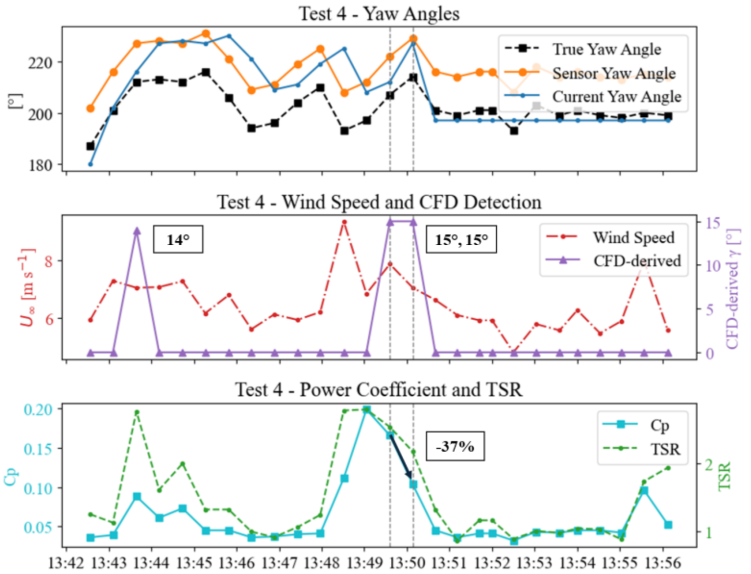

Figure 11. Time series from Test 4: detection of −15° fault and recovery sequence.

3.4 Accuracy evaluation metrics

Table 2 summarizes the performance of the DT model during the third trial, where three out of four tests were subjected to artificially introduced yaw faults. The DT successfully identified misalignment conditions in all faulted cases, with a 100 % detection success rate. Yaw correction accuracy, as the absolute difference between estimated and true yaw errors, was highly accurate, with errors between 0° and 3°, verifying the effectiveness of the inference model.

Large recoveries in Cp were observed after corrective action, such as a +112 % recovery in Test 2. In Test 4, an incorrect initial actuation resulted in a −37 % drop, necessitating a second corrective action, though further recovery was masked by falling wind speed.

Table 2. Evaluation of yaw detection and correction performance using the DT during the third experimental trial.

Metric	Definition	Evaluation Based on Tests
Detection Success Rate	Percentage of faulted tests in which the CFD interpolation detected yaw misalignment ($\gamma \geq 5°$).	3 out of 3 faulted tests: **100 %**
Yaw Correction Accuracy	$\lvert \gamma_{inferred} - \gamma_{true} \rvert$	Test 2 (first feedback): **3°** Test 2 (second feedback): **3°** Test 4: **0°**
Cp Recovery (%)	Percent increase in Cp following yaw correction (when applicable).	Test 2 (first feedback): +**112 %** Test 2 (second feedback): **+17 %** Test 4: **−37 %** after mis-actuation, followed by a recovery attempt, but with an unclear signal due to wind drop.

4 Conclusions

Concept and contribution: This study introduced a DT-based model that, unlike purely data-driven approaches, combines CFD-based performance data with real-time sensor data to identify and correct yaw misalignment caused by flawed wind direction measurements in a small-scale HAWT. By directly determining yaw error from high-fidelity simulation data, rather than assuming accurate inputs from the wind vane, the model enhances operating robustness without requiring new hardware or pre-training on faulted scenarios.

Physical basis and implementation: CFD simulations spanning yaw errors and wind speeds were used to obtain a Cp-TSR-γ performance space of the selected HAWT (with aerodynamic similarity leveraged to reduce dimensionality). A calibration step mapped electromechanical readings to CFD Cp results, and a piecewise-cubic interpolant enabled right-time yaw inference. When the wind vane was flagged as unreliable, the CFD interpolation acted as a virtual sensor to sustain alignment.

Validation under actual conditions: Outdoor trials with injected positive/negative wind vane biases showed that the DT-based model accurately detected and responded to multiple injected yaw faults with a 100 % rate of detection success across faulted tests and achieved yaw correction errors of as low as 0-3°. Cp recovery was as high as +112 % after corrective action, showing considerable recovery of performance.

Practical implications: The approach improves fault tolerance and preserves energy harvesting without LiDAR or additional instrumentation, facilitating SCADA-based analytics and offering a physics-informed route to condition monitoring and sustainable assets management.

Future extensions: Extend the CFD analysis to dynamic yaw misalignment, measure AEP gains and load effects over longer-duration campaigns, strengthen the logic of resolving signs, and generalize the DT-based model to other failures of interest (e.g., leading edge roughness effects, torque/anomaly pitch) through enlarged performance surfaces.

Code availability. Codes generated and used in this research are not available because of confidentiality demands by the corresponding author's company sponsoring the PhD. The codes can be made available by the corresponding author upon reasonable request, with the permission of the company.

Data availability. The dataset generated in this study is not publicly available due to the same reasons of confidentiality. They can be shared by the corresponding author for academic purposes upon request, subject to the approval of the company beforehand.

Author contributions. LC conducted the study, designed and performed all CFD simulations, deployed the DT platform, developed the experimental setup, performed the analyses, and wrote the manuscript. ST advised on technical matters of Digital Twin theory, Arduino integration, and reviewed the manuscript. MML offered engineering insights from an industrial perspective, reviewed experimental design and outcomes. MM organized the collaboration with Cranfield University, granted access to Italian Institute of Welding resources, and reviewed the final manuscript. CC organized the work, reviewed the application of the CFD model, and reviewed the final manuscript.

Competing interests. The authors declare that they have no conflict of interest.

Acknowledgements. The authors acknowledge the support of Cranfield University for hosting the research activities and providing access to laboratory facilities, and the Italian Institute of Welding (Istituto Italiano della Saldatura) for supplying sensors and materials used in the experimental campaign. The authors also thank the Centre for Digital Engineering and Manufacturing (CDEM) of Cranfield University for the technical support and helpful discussions made available during the development of the project. We acknowledge the use of OpenAI's ChatGPT in helping to improve the writing style of this paper.

https://doi.org/10.5194/wes-2025-216
Preprint. Discussion started: 10 December 2025

References

Al-Ttowi, A., Mohammed, A. N., Al-Alimi, S., Zhou, W., Saif, Y., and Ismail, I. F.: Computational Fluid Dynamics (CFD) Investigation of NREL Phase VI Wind Turbine Performance Using Various Turbulence Models, Processes 2024, Vol. 12, Page 1994, 12, 1994, https://doi.org/10.3390/PR12091994, 2024.

ANSYS FLUENT 12.0 Theory Guide - 2.3.1 The Multiple Reference Frame Model: https://www.afs.enea.it/project/neptunius/docs/fluent/html/th/node33.htm#mrf-formulation, last access: 13 October 2025.

MongoDB Atlas | The Modern, Multi-Cloud Database | MongoDB: https://www.mongodb.com/products/platform, last access: 13 October 2025.

Arshad, M. and O'Kelly, B.: Global status of wind power generation: theory, practice, and challenges, Int J Green Energy, 16, 1073–1090, https://doi.org/10.1080/15435075.2019.1597369, 2019.

Astolfi, D., Castellani, F., Becchetti, M., Lombardi, A., and Terzi, L.: Wind Turbine Systematic Yaw Error: Operation Data Analysis Techniques for Detecting It and Assessing Its Performance Impact, Energies 2020, Vol. 13, Page 2351, 13, 2351, https://doi.org/10.3390/EN13092351, 2020.

Astolfi, D., Gao, L., Pandit, R., and Hong, J.: Experimental Analysis of the Effect of Static Yaw Error on Wind Turbine Nacelle Anemometer Measurements, Proceedings - 2023 IEEE International Conference on Environment and Electrical Engineering and 2023 IEEE Industrial and Commercial Power Systems Europe, EEEIC / I and CPS Europe 2023, https://doi.org/10.1109/EEEIC/ICPSEUROPE57605.2023.10194644, 2023.

Badihi, H., Zhang, Y., Jiang, B., Pillay, P., and Rakheja, S.: A Comprehensive Review on Signal-Based and Model-Based Condition Monitoring of Wind Turbines: Fault Diagnosis and Lifetime Prognosis, Proceedings of the IEEE, 110, 754–806, https://doi.org/10.1109/JPROC.2022.3171691, 2022.

Bao, Y. and Yang, Q.: A Data-Mining Compensation Approach for Yaw Misalignment on Wind Turbine, IEEE Trans Industr Inform, 17, 8154–8164, https://doi.org/10.1109/TII.2021.3065702, 2021.

Bashir, M. B. A.: Principle Parameters and Environmental Impacts that Affect the Performance of Wind Turbine: An Overview, Arab J Sci Eng, 47, 7891–7909, https://doi.org/10.1007/S13369-021-06357-1/FIGURES/12, 2022.

Benbouzid, M., Berghout, T., Sarma, N., Djurović, S., Wu, Y., and Ma, X.: Intelligent Condition Monitoring of Wind Power Systems: State of the Art Review, Energies 2021, Vol. 14, Page 5967, 14, 5967, https://doi.org/10.3390/EN14185967, 2021.

Cardaun, M., Roscher, B., Schelenz, R., and Jacobs, G.: Analysis of Wind-Turbine Main Bearing Loads Due to Constant Yaw Misalignments over a 20 Years Timespan, Energies 2019, Vol. 12, Page 1768, 12, 1768, https://doi.org/10.3390/EN12091768, 2019.

Carrattieri, L., Cravero, C., Marsano, D., Valenti, E., Sishtla, V., and Halbe, C.: The Development of Machine Learning Models for Radial Compressor Monitoring With Instability Detection, J Turbomach, 147, https://doi.org/10.1115/1.4066918, 2025.

https://doi.org/10.5194/wes-2025-216
Preprint. Discussion started: 10 December 2025

Chen, P., Lin, Z., Xie, Z., and Qu, C.: Real-time yaw-misalignment calibration and field-test verification of wind turbine via machine learning methods, Mech Syst Signal Process, 208, https://doi.org/10.1016/J.YMSSP.2023.110972, 2024.

Cravero, C., Leutcha, P. J., and Marsano, D.: Development of an analytical model to evaluate the effect of the ported shroud on centrifugal compressors, Green Energy and Intelligent Transportation, 4, 100249, https://doi.org/10.1016/J.GEITS.2024.100249, 2025.

Duranay, Z. B., Güldemir, H., and Coşkun, B.: The Role of Wind Turbine Siting in Achieving Sustainable Energy Goals, Processes, 12, https://doi.org/10.3390/PR12122900, 2024.

Farina, A. and Anctil, A.: Material consumption and environmental impact of wind turbines in the USA and globally, Resour Conserv Recycl, 176, 105938, https://doi.org/10.1016/J.RESCONREC.2021.105938, 2022.

Gao, L. and Hong, J.: Data-driven yaw misalignment correction for utility-scale wind turbines, Journal of Renewable and Sustainable Energy, 13, https://doi.org/10.1063/5.0056671, 2021.

Hulsman, P., Sucameli, C., Petrovi´c, V. P., Rott, A., Gerds, A., and Kühn, M.: The Science of Making Torque from Wind (Turbine power loss during yaw-misaligned free field tests at different atmospheric conditions, TORQUE 2022) Journal of Physics: Conference Series, 2265, 32074, https://doi.org/10.1088/1742-6596/2265/3/032074, 2022.

INTERNATIONAL ELECTROTECHNICAL COMMISSION: IEC 61400-12-1:2022 International Standard Norm, https://www.boutique.afnor.org/fr-fr/norme/iec-614001212022/systemes-de-generation-denergie-eolienne-partie-121-mesures-de-performance-/xs142003/332674, last access: 13 October 2025, 2022.

Jha, S., Jayakumar, G., Abdulgafoor, C. P., Vadlamani, N. R., and Ghosh, S.: CFD predictions of the aerodynamic characteristics of S1223 airfoil at low Reynolds' number, AIAA Aviation Forum and ASCEND, 2024, https://doi.org/10.2514/6.2024-4431, 2024.

Jing, B., Qian, Z., Pei, Y., Zhang, L., and Yang, T.: Improving wind turbine efficiency through detection and calibration of yaw misalignment, Renew Energy, 160, 1217–1227, https://doi.org/10.1016/J.RENENE.2020.07.063, 2020.

Kang, S.-H. ;, Choi, D.-K. ;, Krzywanski, J., Grabowska, K., Skrobek, D., Uddin, G. M., Kang, S.-H., Choi, D.-K., Son, S.-M., and Choi, C.: Generation and Validation of CFD-Based ROMs for Real-Time Temperature Control in the Main Control Room of Nuclear Power Plants, Energies 2024, Vol. 17, Page 6406, 17, 6406, https://doi.org/10.3390/EN17246406, 2024.

Khan, P. W. and Byun, Y. C.: A Review of machine learning techniques for wind turbine's fault detection, diagnosis, and prognosis, Int J Green Energy, 21, 771–786, https://doi.org/10.1080/15435075.2023.2217901, 2023.

Kini, K. R., Harrou, F., Madakyaru, M., and Sun, Y.: Enhancing Wind Turbine Performance: Statistical Detection of Sensor Faults Based on Improved Dynamic Independent Component Analysis, Energies 2023, Vol. 16, Page 5793, 16, 5793, https://doi.org/10.3390/EN16155793, 2023.

De Kooning, J. D. M., Stockman, K., De Maeyer, J., Jarquin-Laguna, A., and Vandevelde, L.: Digital Twins for Wind Energy Conversion Systems: A Literature Review of Potential Modelling Techniques Focused on Model Fidelity and Computational Load, Processes 2021, Vol. 9, Page 2224, 9, 2224, https://doi.org/10.3390/PR9122224, 2021.

Liew, J., Urbán, A. M., and Andersen, S. J.: Analytical model for the power-yaw sensitivity of wind turbines operating in full wake, Wind Energy Science, 5, 427–437, https://doi.org/10.5194/wes-5-427-2020, 2020.

Liu, W. X., Yin, R. P., and Zhu, P. Y.: Deep Learning Approach for Sensor Data Prediction and Sensor Fault Diagnosis in Wind Turbine Blade, IEEE Access, 10, 117225–117234, https://doi.org/10.1109/ACCESS.2022.3219480, 2022.

Lu, J., Li, C., Li, X., Liu, H., Zhang, G., Liu, N., and Liu, L.: Analytical model for the power production of a yaw-misaligned wind turbine, Physics of Fluids, 35, https://doi.org/10.1063/5.0174267/2929442, 2023.

Momber, A. W., Möller, T., Langenkämper, D., Nattkemper, T. W., and Brün, D.: A Digital Twin concept for the prescriptive maintenance of protective coating systems on wind turbine structures, Wind Engineering, 46, 949–971, https://doi.org/10.1177/0309524X211060550, 2022.

Muiruri, P. I., Motsamai, O. S., and Ndeda, R.: A comparative study of RANS-based turbulence models for an upscale wind turbine blade, SN Appl Sci, 1, 1–15, https://doi.org/10.1007/S42452-019-0254-5/FIGURES/15, 2019.

Shakya, P., Thomas, M., Seibi, A. C., Shekaramiz, M., and Masoum, M. A. S.: Fluid-structure interaction and life prediction of small-scale damaged horizontal axis wind turbine blades, Results in Engineering, 23, 102388, https://doi.org/10.1016/J.RINENG.2024.102388, 2024.

Siddiqui, M. S., Rasheed, A., Tabib, M., and Kvamsdal, T.: Numerical investigation of modeling frameworks and geometric approximations on NREL 5 MW wind turbine, Renew Energy, 132, 1058–1075, https://doi.org/10.1016/J.RENENE.2018.07.062, 2019.

Siddiqui, M. S., Khalid, M. H., Badar, A. W., Saeed, M., and Asim, T.: Parametric Analysis Using CFD to Study the Impact of Geometric and Numerical Modeling on the Performance of a Small Scale Horizontal Axis Wind Turbine, Energies 2022, Vol. 15, Page 505, 15, 505, https://doi.org/10.3390/EN15020505, 2022.

Simley, E., Bortolotti, P., Scholbrock, A., Schlipf, D., and Dykes, K.: IEA Wind Task 32 and Task 37: Optimizing Wind Turbines with Lidar-Assisted Control Using Systems Engineering, J Phys Conf Ser, 1618, 042029, https://doi.org/10.1088/1742-6596/1618/4/042029, 2020.

Solari, F., Lysova, N., and Montanari, R.: Monitoring and control of air filtration systems: Digital twin based on 1D computational fluid dynamics simulation and experimental data, Comput Ind Eng, 197, 110607, https://doi.org/10.1016/J.CIE.2024.110607, 2024.

Stadtmann, F., Rasheed, A., Kvamsdal, T., Johannessen, K. A., San, O., Kolle, K., Tande, J. O., Barstad, I., Benhamou, A., Brathaug, T., Christiansen, T., Firle, A. L., Fjeldly, A., Froyd, L., Gleim, A., Hoiberget, A., Meissner, C., Nygard, G., Olsen, J., Paulshus, H., Rasmussen, T., Rishoff, E., Scibilia, F., and Skogas, J. O.: Digital Twins in Wind Energy: Emerging Technologies and Industry-Informed Future Directions, IEEE Access, 11, 110762–110795, https://doi.org/10.1109/ACCESS.2023.3321320, 2023.

Veers, P., Dykes, K., Basu, S., Bianchini, A., Clifton, A., Green, P., Holttinen, H., Kitzing, L., Kosovic, B., Lundquist, J. K., Meyers, J., O'malley, M., Shaw, W. J., and Straw, B.: Grand Challenges: wind energy research needs for a global energy transition, Wind Energy Science, 7, 2491–2496, https://doi.org/10.5194/wes-7-2491-2022, 2022.

Virtanen, P., Gommers, R., Oliphant, T. E., Haberland, M., Reddy, T., Cournapeau, D., Burovski, E., Peterson, P., Weckesser, W., Bright, J., van der Walt, S. J., Brett, M., Wilson, J., Millman, K. J., Mayorov, N., Nelson, A. R. J., Jones, E., Kern, R., Larson, E., Carey, C. J., Polat, İ., Feng, Y., Moore, E. W., VanderPlas, J., Laxalde, D., Perktold, J., Cimrman, R., Henriksen, I., Quintero, E. A., Harris, C. R., Archibald, A. M., Ribeiro, A. H., Pedregosa, F., van Mulbregt, P., Vijaykumar, A., Bardelli, A. Pietro, Rothberg, A., Hilboll, A., Kloeckner, A., Scopatz, A., Lee, A., Rokem, A., Woods, C. N., Fulton, C., Masson, C., Häggström, C., Fitzgerald, C., Nicholson, D. A., Hagen, D. R., Pasechnik, D. V., Olivetti, E., Martin, E., Wieser, E., Silva, F., Lenders, F., Wilhelm, F., Young, G., Price, G. A., Ingold, G. L., Allen, G. E., Lee, G. R., Audren, H., Probst, I., Dietrich, J. P., Silterra, J., Webber, J. T., Slavič, J., Nothman, J., Buchner, J., Kulick, J., Schönberger, J. L., de Miranda Cardoso, J. V., Reimer, J., Harrington, J., Rodríguez, J. L. C., Nunez-Iglesias, J., Kuczynski, J., Tritz, K., Thoma, M., Newville, M., Kümmerer, M., Bolingbroke, M., Tartre, M., Pak, M., Smith, N. J., Nowaczyk, N., Shebanov, N., Pavlyk, O., Brodtkorb, P. A., Lee, P., McGibbon, R. T., Feldbauer, R., Lewis, S., Tygier, S., Sievert, S., Vigna, S., Peterson, S., More, S., Pudlik, T., et al.: SciPy 1.0: fundamental algorithms for scientific computing in Python, Nat Methods, 17, 261–272, https://doi.org/10.1038/S41592-019-0686-2;SUBJMETA, 2020.

Wang, X., Ye, Z., Kang, S., and Hu, H.: Investigations on the Unsteady Aerodynamic Characteristics of a Horizontal-Axis Wind Turbine during Dynamic Yaw Processes, Energies 2019, Vol. 12, Page 3124, 12, 3124, https://doi.org/10.3390/EN12163124, 2019.

Yusong, Y. and Solomin, E.: The Control Strategy and Simulation of the Yaw System for MW Rated Wind Turbine, Proceedings - 2020 Russian Workshop on Power Engineering and Automation of Metallurgy Industry: Research and Practice, PEAMI 2020, 87–92, https://doi.org/10.1109/PEAMI49900.2020.9234343, 2020.